

# Macroscopic neutrinoless double beta decay: long range quantum coherence

Gordon Baym and Jen-Chieh Peng

*Illinois Center for Advanced Studies of the Universe  
and Department of Physics, University of Illinois, 1110 W. Green Street, Urbana, IL 61801*

(Dated: March 19, 2024)

We re-introduce, in light of our modern understanding of neutrinos, the concept of “macroscopic neutrinoless double beta decay” (MDBD) for Majorana neutrinos. In this process an antineutrino produced by a nucleus undergoing beta decay,  $X \rightarrow Y + e^- + \bar{\nu}_e$ , is absorbed as a neutrino by another identical  $X$  nucleus via the inverse beta decay reaction,  $\nu_e + X \rightarrow e^- + Y$ . The distinct signature of MDBD is that the total kinetic energy of the two electrons equals twice the endpoint energy of single beta decay. The amplitude for MDBD, a coherent sum over the contribution of different mass states of the intermediate neutrinos, reflects quantum coherence over macroscopic distances, and is a new macroscopic quantum effect. We evaluate the rate of MDBD for a macroscopic sample of “ $X$ ” material, e.g., tritium, acting both as the source and the target. The accidental background for MDBD originating from two separate single beta decays, which contains two final state neutrinos, can be readily rejected by measuring the energy of the detected two electrons. We discuss the similarities and differences between the MDBD and conventional neutrinoless double beta decay.

PACS numbers:

## I. INTRODUCTION

The neutrino, if a Majorana rather than a Dirac fermion, would be its own antiparticle. A key experimental signature distinguishing Majorana neutrinos from Dirac neutrinos is nuclear neutrinoless double beta decay ( $0\nu\text{DBD}$ ) [1],

$$(A, Z) \rightarrow (A, Z + 2) + e^- + e^-. \quad (1)$$

Despite the importance of determining whether neutrinos are Majorana or Dirac, and despite a major experimental effort, only upper limits for  $0\nu\text{DBD}$  have so far been obtained [2–4]. Ongoing and future experiments with multi-ton detectors will further improve the sensitivity in these searches [5].

The existence of a Majorana neutrino implies lepton-number non-conservation, hence physics beyond the Standard Model. Majorana neutrinos have only two spin states: when massless the left-handed state is a neutrino and the right-handed an antineutrino. The “sea-saw” mechanism for Majorana neutrinos can then provide a natural explanation for the very light neutrino masses inferred from tritium beta decay (TBD) and neutrino oscillation experiments [6].

The standard picture of neutrinoless double beta decay is that the *antineutrino* emitted from a neutron in a nucleus is absorbed as a *neutrino* on a neutron in the same nucleus. But there is in general no requirement in neutrinoless double beta decay that the second neutron be in the same nucleus – as was recognized early in Ref. [7] (and followed up in Refs. [8, 9]) – or indeed that the second nucleus be the same nuclide as the first, or even that the two down quarks undergoing weak interactions be in different neutrons. In this paper, we analyze in detail the concept of “macroscopic neutrinoless double beta decay” (MDBD), in which a Majorana neutrino emitted

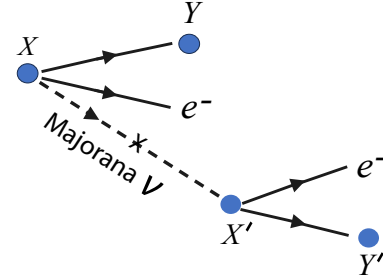


FIG. 1: Illustration of macroscopic neutrinoless double beta decay, with time running to the right. The first nucleus,  $X$  undergoes a beta decay emitting an electron and a Majorana antineutrino, which is absorbed as a neutrino by a second nucleus  $X'$  in an inverse beta decay. The sum of the energies of the two electron emitted is just the sum of the individual endpoint energies in the beta decays of  $X$  and  $X'$ .

from one nucleus is absorbed in a second nucleus. For example, in the single beta decay (XBD) from parent nucleus  $X = (A, Z)$  to daughter nucleus  $Y = (A, Z + 1)$ ,

$$X \rightarrow Y + e^- + \bar{\nu}_e, \quad (2)$$

the antineutrino produced is, for Dirac type neutrinos, distinct from  $\nu_e$  and cannot participate in the inverse beta decay (IXBD) reaction

$$\nu_e + X \rightarrow e^- + Y; \quad (3)$$

the nucleus  $X$  can only absorb an electron neutrino,  $\nu_e$ , to reach the final state  $e^- + Y$ . If neutrinos are Majorana however, then the neutrino and antineutrino are not distinct particles, and the antineutrino in the XBD can then participate in the IXBD. The combination of these

two sequential reactions, (2) and (3), is the macroscopic neutrinoless double beta decay, illustrated in Fig. 1,

$$X + X' \rightarrow Y + Y' + e^- + e^-, \quad (4)$$

where we add a prime to indicate the freedom of the two nuclei being different nuclides. This process is the macroscopic analog of the conventional neutrinoless double beta decay,  $0\nu\text{DBD}$ . Both decays effectively turn two neutrons into two protons plus two electrons. Both decays violate lepton number conservation and require the neutrino to be Majorana.

Detection of neutrinoless double beta decay, whether in a single nucleus or via MDBD exchange of a non-zero mass Majorana neutrino between different nuclei would violate lepton number conservation and would establish that neutrinos are Majorana and not Dirac. In neutrinoless double beta decay the initial and final nuclei (or quarks more precisely) exchange a Majorana neutrino in various mass states. An important aspect of this exchange is the possibility of quantum interference between neutrino exchange in different mass states. This interference is implicitly included in calculation of microscopic  $0\nu\text{DBD}$  [2]. Macroscopic beta decay, however, opens new quantum interference effects over the macroscopic distance scales of the separation between source and target nuclei.

The two processes have notable differences. All  $\beta$ -unstable nuclei are potential candidates for MDBD, while only a limited number of nuclei are candidates for  $0\nu\text{DBD}$ . The uncertainties in the rate of MDBD are considerably smaller than in  $0\nu\text{DBD}$ . In  $0\nu\text{DBD}$  within a single nucleus, the uncertainty in the matrix elements [10, 11] owes both to the many processes within the standard model that can contribute to the decay, e.g.,  $n \rightarrow \Delta^{++} + 2e$ , where the  $\Delta^{++}$  lives virtually, as well as exchanges of virtual particles beyond the standard model in addition to Majorana neutrino exchange. Beyond-the-standard-model physics that could lead to  $0\nu\text{DBD}$  include right-handed weak currents, exchange of heavy neutrinos or supersymmetric particles, etc.<sup>1</sup> By contrast, MDBD must come only from light massive Majorana neutrinos. Moreover, the matrix elements for sequential beta and inverse beta decay reactions in MDBD are precisely known.

Not only does the antineutrino source in neutrinoless MDBD not need to be the same nucleus as the target, the antineutrino emitted, as we detail later, does not need even to be an electron type. For example in  $\pi^- \rightarrow \mu^- + \bar{\nu}_\mu$ , the muon antineutrino, if Majorana, can be absorbed as an electron neutrino in an inverse beta decay.

In addition, while the  $0\nu\text{DBD}$  rate is insensitive to the geometry of the source and is linearly proportional to

the source mass, the rate for MDBD rate, as we spell out below, depends sensitively on the geometry of the source and is proportional to the source mass to the 4/3 power.

We emphasize that we do not consider MDBD as a replacement for traditional  $0\nu\text{DBD}$  experiments. While we calculate yields for several model MDBD systems, realistic experiments with radioactive nuclei are not feasible at the moment. Nonetheless the concept of MDBD should stimulate new ways of looking at neutrinoless weak interactions.

In the next Section, II, we first review the calculation of the rate of single beta decay, and the cross section for inverse beta decay. In Sec. III we derive the rate of MDBD as a coherent quantum process between the initial single beta decay and the inverse beta decay, and derive the dependence of the MDBD rate on the geometry of the source. Then in Sec. IV we discuss how the MDBD signal is readily differentiated from the experimental two electron backgrounds. We conclude in Sec. V.

## II. BETA AND INVERSE BETA DECAY WITH MASSIVE NEUTRINOS

In this section we first review the role of chirality and helicity for massive neutrinos in beta and inverse beta decay. We then briefly review the rates for emission of an antineutrino of given helicity in beta decay and the absorption of a neutrino of given helicity in inverse beta decay.

### A. Chirality and helicity

Eigenstates of  $\gamma_5$  have definite chirality; we denote the  $\gamma_5$  eigenvalue in these states as *positive* ( $\gamma_5 = 1$ ) or *negative* ( $\gamma_5 = -1$ ). While chirality and helicity (the eigenvalue  $h$  of the projection of the spin direction along the direction of motion,  $\hat{\Sigma} \cdot \hat{p}$ ) coincide for massless neutrinos, where a positive chirality state always has positive helicity,  $h=1$ , and a negative chirality state always has negative helicity  $h=-1$ , they are not the same for finite mass neutrinos. We denote positive helicity as *right handed*, and negative helicity as *left handed*.

In beta decay, antineutrinos are emitted with positive chirality,  $\gamma_5 = 1$ , while neutrinos can be absorbed in the inverse reaction only if they have negative chirality. Neutrinos are preferentially absorbed with helicity opposite to that of the antineutrino in beta decay. Since chirality is conserved for massless neutrinos, a massless Majorana antineutrino emitted in beta decay has the wrong chirality ever to be absorbed as a neutrino; both MDBD and  $0\nu\text{DBD}$  are forbidden.

Independent of the neutrino mass, however, neutrinos and antineutrinos, in the absence of external forces, e.g., gravitational [14] or magnetic [15], propagate in states of definite helicity. When neutrinos have finite mass, chirality is no longer a constant of the motion,

<sup>1</sup> Nonetheless, even if such processes were to underlie  $0\nu\text{DBD}$ , the observation of such double beta decays would establish that the neutrino is Majorana [12, 13].

since  $\gamma_5$  does not commute with the mass term in the Hamiltonian. In detail, as reviewed in the Appendix, an antineutrino emitted with positive chirality has amplitude  $\alpha^\pm = \sqrt{(1 \pm \beta_\nu)/2}$  to be right or left handed, where  $\beta_\nu = v_\nu/c$ , with  $v_\nu$  the neutrino velocity. Similarly, a right or left handed neutrino has amplitude  $\sqrt{(1 \mp \beta_\nu)/2} = \alpha^\mp$  to have the negative chirality needed to be absorbed in an inverse beta decay. Thus a Majorana neutrino effectively has a total amplitude for emission with positive chirality and absorption with negative chirality, summed over both intermediate helicities,  $\alpha^+ \alpha^- + \alpha^- \alpha^+ = \sqrt{1 - \beta_\nu^2} = m_\nu/E_\nu$ , where  $m_\nu$  and  $E_\nu$  are the neutrino mass and energy. States of definite helicity have amplitudes to be of either chirality, thus allowing neutrinoless double beta decay for finite mass Majorana neutrinos.

### B. Single beta decay

We now discuss the amplitude,  $\mathcal{A}_{BD}^{ih}$ , and then the rate of beta decay, (2), with emission of a  $\bar{\nu}_e$  in mass state  $i$  and helicity  $h$ , neglecting nuclear recoil (a better and better approximation the heavier the parent nucleus). The amplitude is

$$\mathcal{A}_{BD}^{ih} = \mathcal{M}_i \alpha_\nu^{ih}. \quad (5)$$

where  $\mathcal{M}_i \propto G_F V_{ud} U_{ei}$ , with  $G_F$  the Fermi weak coupling constant,  $V_{ud} = 0.97425$  the Cabbibo-Kobayashi-Maskawa (CKM) up-down quark matrix element, and  $U_{ei}$  the Pontecorvo-Maki-Nakagawa-Sakata (PMNS) neutrino mixing matrix element. For right and left antineutrino helicities,  $\alpha_\nu^{i,h=\pm 1} = \alpha^\pm$ . For given neutrino energy,  $\beta_i$  depends on the neutrino mass,  $m_i$ ; since for  $m_i \ll E_{\nu i}$ ,  $\beta_i \simeq 1 - m_i^2/2E_{\nu i}^2$ ,

$$\alpha_\nu^{iR} \simeq 1, \quad \alpha_\nu^{iL} \simeq \frac{m_i}{2E_{\nu i}}. \quad (6)$$

The dependence on the neutrino mass state is through the factors  $U_{ei}$  and  $\alpha_\nu^{ih}$ , and the helicity dependence resides in  $\alpha_\nu^{ih}$ .

The full squared matrix element has the form

$$|\mathcal{M}_i|^2 = 2\pi W(E_e) |U_{ei}|^2, \quad (7)$$

where for tritium for example [16, 17],

$$W(E_e) = \frac{G_F^2}{2\pi} |V_{ud}|^2 F(Z, E_e) (m_{3He}/m_{3H}) |M_f|^2, \quad (8)$$

with  $F(Z, E_e)$  the Fermi Coulomb factor for the electron- $^3\text{He}$  system, and  $|M_f|^2$  the sum of the nuclear form factors for Fermi and Gamow-Teller transitions.<sup>2</sup> In further

calculation we symbolically write the matrix element as  $\mathcal{M}_i = \sqrt{2\pi} W U_{ei}$ .

The rate of beta decay with emission of a neutrino of given helicity is then

$$d\Gamma_{XBD}^h = \sum_i \frac{d^3 p_\nu}{(2\pi)^3} \frac{d^3 p_e}{(2\pi)^3} 2\pi |\mathcal{M}_i|^2 (\alpha_\nu^{ih})^2 \delta(\Delta M - E_e - E_{\nu i}), \quad (9)$$

where  $\Delta M = m_X - m_Y$  is the total energy released in the beta decay.

Integrating over all electron states, and writing  $d^3 p_\nu = 4\pi p_\nu E_\nu dE_\nu$ , we have

$$\frac{d\Gamma_{XBD}^h}{dE_\nu} = \frac{\bar{\sigma}(E_e)}{2\pi^2} \sum_i |U_{ei}|^2 (1 + h\beta_i) E_\nu \sqrt{E_\nu^2 - m_i^2}, \quad (10)$$

where  $E_e = \Delta M - E_\nu$  and

$$\bar{\sigma}(E_e) \equiv p_e E_e W(E_e). \quad (11)$$

The differential rate of beta decay, for  $m_i \ll E_\nu$ , summed over  $h$  and using  $\sum_i |U_{ei}|^2 = 1$ , is

$$\frac{d\Gamma_{XBD}}{dE_\nu} \simeq \frac{\bar{\sigma}(E_e)}{\pi^2} E_\nu^2. \quad (12)$$

For tritium, in the limit of a zero energy neutrino [16],  $\bar{\sigma} \simeq 3.834 \times 10^{-45} \text{ cm}^2$ . The inverse of the mean lifetime,  $\tau$ , of the nucleus  $X$  against beta decay (17.8 yr for tritium) is then  $\int dE_\nu (d\Gamma_{XBD}/dE_\nu)$ .

### C. Inverse beta decay

While the rate of beta decay is an incoherent sum over the mass states in the emitted antineutrino, the rate of inverse beta decay depends strongly on the nature of the neutrino impinging on the target nucleus. For example, neutrinos from the Big Bang arrive at Earth in definite mass eigenstates, a result of the spatial separation of the mass components of a neutrino wavepacket caused by the dependence of the neutrino velocity on the mass state. By contrast, neutrinos from nuclear weak interactions, in  $^{51}\text{Cr}$  for example [18], are emitted in pure electron neutrino flavor states. These neutrinos can initiate inverse beta decay whether the neutrino is Dirac or Majorana. On the other hand, antineutrinos can participate in inverse beta decay (with electron emission) only if the neutrino is Majorana. These antineutrinos can be either in mass eigenstates, e.g., if they come from the Big Bang, or in flavor eigenstates, e.g., from tritium beta decay or a nuclear power plant. If the incident neutrino was emitted as a Majorana antineutrino, the amplitude for inverse beta decay is a coherent sum over the mass eigenstates in the neutrino.

<sup>2</sup> For tritium,  $|M_f|^2 = 1 + 2.788(g_A/g_V)^2$ , with  $(g_A/g_V)^2 = 1.6116$ , while for the neutron,  $|M_f|^2 = 1 + 3(g_A/g_V)^2$ .

Common to all these processes is the inverse beta decay amplitude for a neutrino in a given mass state. Specifically, the amplitude,  $\mathcal{A}_{IXBD}^{ih}$ , for inverse beta decay induced by a neutrino with velocity  $\beta_i$ , mass  $m_i$  and helicity  $h$  incident on a target nucleus, is

$$\mathcal{A}_{IXBD}^{ih} = \mathcal{M}_i \alpha_\nu^{ih}, \quad (13)$$

where  $\alpha_\nu^{ih} = \sqrt{(1 - h\beta_i)/2}$ , with  $\mathcal{M}_i$  the same as before.

The cross section for inverse beta decay for an incident neutrino in a given mass state  $i$  and helicity  $h$  is similarly (cf. Eq. (9)),

$$\begin{aligned} \frac{d\sigma_{IXBD}^{ih}}{d\Omega_e} &= \int \frac{p_e^2 dp_e}{(2\pi)^2} |\mathcal{M}_i|^2 (\alpha_\nu^{ih})^2 \delta(m_X + E_\nu - m_Y - E_e) \\ &= \frac{p_e E_e}{(2\pi)^2} |\mathcal{M}_i|^2 (\alpha_\nu^{ih})^2 = \frac{\bar{\sigma}(E_e)}{4\pi} |U_{ei}|^2 (1 - h\beta_i), \end{aligned} \quad (14)$$

and the total IXBD cross section  $\sigma_{IXBD}^{ih}$  equals  $\bar{\sigma}|U_{ei}|^2(1 - h\beta_i)$ . As in beta decay, the helicity dependence is in the factor  $\alpha_\nu^{ih}$ . The scale of both the lifetime of a nucleus under beta decay, and the IXBD cross section is set by  $\bar{\sigma}(E_e)$ .

If the initial neutrino is fully relativistic in mass state  $i$  ( $\beta_\nu \rightarrow 1$ ), then only the left handed helicity component can lead to emission of an electron, and the cross section for an incident mass state  $i$  is  $2\bar{\sigma}|U_{ei}|^2$ . (Were the initial neutrino in an incoherent sum over mass states  $i$ , the cross section would become  $2\bar{\sigma}$ .) But for slowly moving relic neutrinos ( $\beta_\nu \rightarrow 0$ ),  $\alpha_\nu^{ih} \rightarrow 1/\sqrt{2}$  and the IXBD amplitude becomes independent of the neutrino helicity. More generally, if the initial neutrino state is a coherent sum of mass states, the rate of IXBD reflects interference between the states, a problem we focus on in calculating the rate of MDBD below.

### III. MACROSCOPIC DOUBLE BETA DECAY

We turn now to calculating the rate of macroscopic double beta decay in terms of the known physics of the single beta decay, XBD, and inverse beta decay, IXBD. The rate of MDBD within a sample of atoms of nucleus  $X$ , with the sample acting both as the source of beta decays as well as the target for inverse beta decays, depends on both the microscopics of XBD and IXBD as well as the geometry of the ensemble of  $X$  atoms present. For spacing between the atoms large compared with the characteristic intermediate neutrino wavelength, the neutrinos can be taken to be on-shell, in contrast to neutrinoless double beta decay within a single nucleus. The MDBD process can take place for either helicity of the intermediate neutrino.

Since the Majorana neutrino in MDBD exists only as an intermediary between the initial electron and final

electron emission processes, the contributions of the different neutrino mass states are coherent, and give rise to quantum interference. To see this effect it is necessary to evaluate the MDBD rate in terms of the total amplitude for the process.

While neutrino oscillations become important in processes over astrophysical distances, e.g., in the sun and in neutron stars, they are insignificant in MDBD over laboratory distances, except for very small neutrino energies. The characteristic length (in meters) in neutrino oscillations for a neutrino of energy  $E_\nu$  (in MeV) is  $L(\text{m})_{osc} \simeq E_\nu(\text{MeV})/\Delta m_{31}^2(\text{eV}^2)$ , where  $\Delta m_{31}^2 = m_3^2 - m_1^2 \simeq 2.5 \times 10^{-3} \text{eV}^2$  corresponds to the difference of the squares of the masses of the heaviest and lightest neutrinos. Thus  $L_{osc} \sim E_\nu(\text{MeV}) \text{ km}$ . Neutrinos of sub-keV energy could undergo neutrino oscillations in MDBD in large samples, but their effect would be hard to observe.

We assume the initial beta decay to take place at point  $\vec{r}$  and the inverse beta decay at  $\vec{r}'$ . The total amplitude for the process  $X + X \rightarrow Y + Y + e^- + e^{-'}$  is

$$\begin{aligned} \mathcal{A}_{MDBD}(\vec{r} - \vec{r}') &= \sum_{ih} \int \frac{d^3 p_\nu}{(2\pi)^3} \frac{(\mathcal{A}_{XBD}^{ih} e^{i(\vec{p}_\nu + \vec{p}_e) \cdot \vec{r}}) (\mathcal{A}_{IXBD}^{ih} e^{i(\vec{p}'_e - \vec{p}_\nu) \cdot \vec{r}'})}{\Delta M - E_e - E_\nu + i\eta}, \end{aligned} \quad (15)$$

where  $\eta \rightarrow 0^+$ . Then using the amplitudes (5) and (13), doing the sum over helicities,

$$\sum_h \alpha_\nu^{ih} \alpha_\nu^{ih} = \sqrt{1 - \beta_i^2} = m_{\nu i}/E_\nu, \quad (16)$$

and the angular integration over the directions of the intermediate neutrino, we have

$$\begin{aligned} \mathcal{A}_{MDBD} &= e^{i(\vec{p}_e \cdot \vec{r} + \vec{p}'_e \cdot \vec{r}')} \frac{\sqrt{W(E_e)W(E'_e)}}{\pi |\vec{r} - \vec{r}'|} \sum_i U_{ei}^2 m_{\nu i} \\ &\times \int \frac{E_\nu dE_\nu \sin(p_\nu |\vec{r} - \vec{r}'|)}{\Delta M - E_e - E_\nu + i\eta}. \end{aligned} \quad (17)$$

For large  $|\vec{r} - \vec{r}'|$  compared with characteristic  $1/p_\nu$ , only the on-shell contribution of the neutrino (from the imaginary part  $-i\pi\delta(X)$  of the denominator term,  $1/(X + i\eta)$ ) is significant. In this macroscopic limit the integral in the lower line of Eq. (17) becomes  $-i\pi E_\nu \sin(p_\nu |\vec{r} - \vec{r}'|)$ , where now  $E_\nu = \Delta M - E_e$ . We drop the overall phase factors, which do not enter the MDBD rate, and finally arrive at the MDBD amplitude,

$$\mathcal{A}_{MDBD} = \sqrt{W(E_e)W(E'_e)} \frac{\sin(p_\nu |\vec{r} - \vec{r}'|)}{|\vec{r} - \vec{r}'|} \sum_i U_{ei}^2 m_{\nu i}. \quad (18)$$

The total rate of MDBD with one emitter and one

absorber is then

$$\Gamma_{MDBD} = \int \frac{d^3 p_e}{(2\pi)^3} \frac{d^3 p'_e}{(2\pi)^3} |\mathcal{A}_{MDBD}|^2 2\pi \delta(2\Delta M - E_e - E'_e). \quad (19)$$

For  $p_\nu |\vec{r} - \vec{r}'| \gg 1$  the  $\sin^2$  factor, slightly cross-grained in  $\vec{r}'$ , becomes  $1/2$ , and thus

$$\Gamma_{MDBD} = \frac{\mathcal{K}}{4\pi |\vec{r} - \vec{r}'|^2}, \quad (20)$$

where the microscopic rate factor, after doing the  $E'_e$  integral, becomes

$$\mathcal{K} = \bar{m}^2 \int \frac{\bar{\sigma}(E_e) \bar{\sigma}(E'_e)}{\pi^2} dE_e. \quad (21)$$

Here  $E'_e = 2\Delta M - E_e$ , and

$$\bar{m} \equiv |\sum_i U_{ei}^2 m_{\nu i}| \quad (22)$$

is the average neutrino mass entering neutrinoless double beta decay.

We can understand the remaining structure of the MDBD rate by considering simply the single mass state contribution, denoted as  $\Gamma_{MDBD}^i$ . The beta decay of an  $X$  nucleus at point  $\vec{r}$  produces a flux, per unit neutrino energy, of neutrinos in helicity state  $h$  of energy  $E_\nu$  at point  $\vec{r}'$ ,

$$\frac{dF^{ih}(\vec{r}')}{dE_{\nu i}} = \frac{1}{4\pi |\vec{r} - \vec{r}'|^2} \frac{d\Gamma_{XBD}^{ih}}{dE_{\nu i}}. \quad (23)$$

Thus the full rate for neutrinos emitted at point  $\vec{r}$  in mass state  $i$  to be absorbed at point  $\vec{r}'$  is

$$\Gamma_{MDBD}^i = \sum_h \int \frac{dF^{ih}(\vec{r}')}{dE_{\nu i}} dE_{\nu i} \sigma_{IXBD}^{ih} = \frac{\mathcal{K}_i}{4\pi |\vec{r} - \vec{r}'|^2}, \quad (24)$$

where

$$\begin{aligned} \mathcal{K}_i &= \int dE_{\nu i} \sum_h \frac{d\Gamma_{XBD}^{ih}}{dE_{\nu i}} \sigma_{IXBD}^{ih} \\ &= |U_{ei}|^4 m_{\nu i}^2 \int dE_{\nu i} \frac{\bar{\sigma}(E_e) \bar{\sigma}(E'_e)}{\pi^2}; \end{aligned} \quad (25)$$

this result is precisely the single neutrino mass state ( $i$ ) contribution to  $\mathcal{K}$ , Eq. (21), with the identifications  $E_e = \Delta M - E_{\nu i}$  and  $E'_e = \Delta M + E_{\nu i} = 2\Delta M - E_e$ .

The integral in  $\mathcal{K}$  depends very weakly on the neutrino masses since  $m_\nu \ll m_e$ , and we neglect them in the integral. Furthermore the  $\bar{\sigma}$  do not vary greatly over the range of neutrino energies, and we write them as  $\bar{\sigma}$  evaluated at the end point energy times a correction. Neglecting the energy dependence in the Fermi Coulomb term,  $F$  in  $\bar{\sigma}$  we have

$$\mathcal{K} = \frac{1}{\pi^2} \bar{m}^2 \bar{\sigma}_{end}^2 K_{end} \mathcal{J}, \quad (26)$$

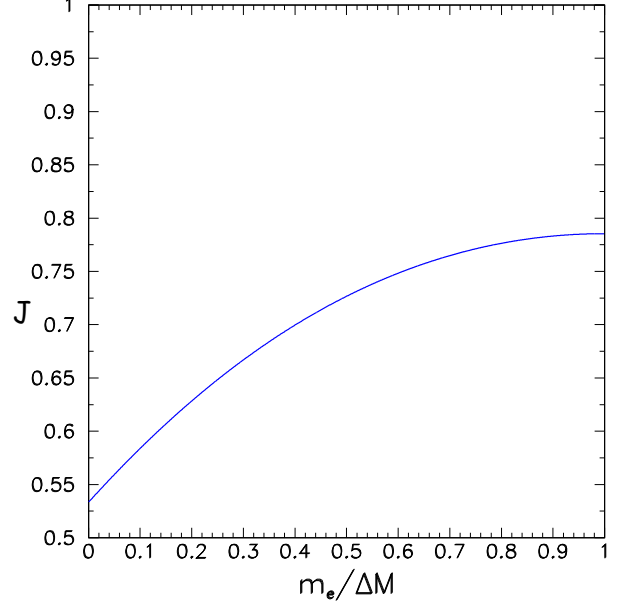


FIG. 2: The dimensionless integral  $\mathcal{J}$  entering the MDBD rate, as a function of  $m_e/\Delta M$ .

where  $K_{end} = \Delta M - m_e$  is the endpoint kinetic energy of the XBD,  $\bar{\sigma}_{end} \equiv \bar{\sigma}(E_e = \Delta M)$ , and the dimensionless factor  $\mathcal{J}$  is given by

$$\mathcal{J}(m_e/\Delta M) = \int_0^{K_{end}} \frac{dE_\nu}{K_{end}} \frac{p_e E_e p'_e E'_e}{(K_{end}^2 - m_e^2) K_{end}^2}. \quad (27)$$

Figure 2 shows  $\mathcal{J}$  as a function of  $m_e/\Delta M$ . In the limit that the Q value in the XBD is small compared with the electron mass, or  $\Delta M - m_e \ll m_e$ , as in tritium, then  $\mathcal{J} \rightarrow \pi/4$  (this factor arises from the averaging of the momenta of the electrons), and

$$\mathcal{K} \rightarrow \frac{\bar{m}^2 \bar{\sigma}_{end}^2}{4\pi} K_{end}. \quad (28)$$

In the opposite limit,  $\Delta M \gg m_e$ , the correction factor  $\mathcal{J}$  becomes  $8/15$ , and  $\mathcal{K} \rightarrow (8\bar{m}^2 \bar{\sigma}_{end}^2 / 15\pi^2) K_{end}$ .

### A. Quantum interference and coherence

The rate of MDBD is proportional to the square of the weighted neutrino mass  $|\sum_i U_{ei}^2 m_{\nu i}|^2$ . This term includes both the direct ( $i = j$ ) MDBD process, with a sum of the rates for single mass eigenstates,  $\sum_i |U_{ei}|^4 m_{\nu i}^2$ , as well as the interference between different mass eigenstates ( $i \neq j$ ). By contrast, if the incident neutrino is an incoherent sum of mass states, then the rate is proportional to the  $i = j$  term alone, i.e.,

$$\sum_i |U_{ei}|^4 m_{\nu i}^2 \equiv m_{incoh}^2, \quad (29)$$



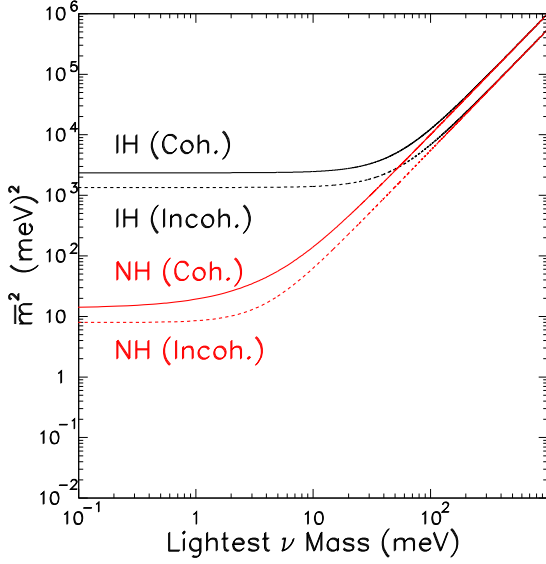


FIG. 3: The calculated  $\bar{m}^2$  for the normal (NH) and inverted (IH) neutrino mass hierarchies with and without interference between the mass eigenstates. The curves labelled “coherent” assume zero Majorana phases (with respect to the CP phase), while the curves labelled “incoherent” neglect the off-diagonal interference between different mass eigenstates. In this case coherence increases  $\bar{m}^2$  and the rate of MDBD.

a very different weighting of the neutrino masses.

The dependence of  $\bar{m}$  on possible phases of the  $U_{ei}$  is a consequence of quantum interference between different mass states  $i$  in macroscopic double beta decay. Explicitly,  $\bar{m}$  can be written in terms of the CP phase  $\delta$  and Majorana phases  $\lambda_a$  and  $\lambda_b$ , as,

$$\bar{m} = \left| |U_{e1}|^2 e^{2i\lambda_a} m_1 + |U_{e2}|^2 e^{2i\lambda_b} m_2 + |U_{e3}|^2 e^{-2i\delta} m_3 \right|. \quad (30)$$

Figure 3 shows  $\bar{m}^2$  as a function of lightest neutrino mass for the normal and inverted mass hierarchies, using the neutrino oscillation parameters tabulated in [21]. The curves labelled “incoherent” neglect the interference terms in  $\bar{m}^2$ , and include only the diagonal sum over mass eigenstates, i.e., with  $\bar{m}^2$  replaced by  $m_{incoh}^2$ . In the curves labelled “coherent,” we assume that the Majorana CP phases equal  $-\delta$ , so that all the phases drop out of  $\bar{m}$ , and  $\bar{m}^2 - m_{incoh}^2 = \sum_{i \neq j} |U_{ei}|^2 |U_{ej}|^2 m_{\nu i} m_{\nu j} > 0$ . In this case, coherence increases the MDBD rate. For given neutrino mass splittings, the curves are in fact simply quadratic functions of the lightest neutrino mass.

On the other hand, if the Majorana CP phases differ from  $-\delta$ , coherence can, as illustrated in Fig. 4, decrease the rate, exactly as in  $0\nu$ DBD [2]. Figure 4 also shows, on the right hand scale, the MDBD rate for a spherical source of 100 g of tritium, calculated from Eq. (33) below.

Macroscopic double beta decay remains coherent as

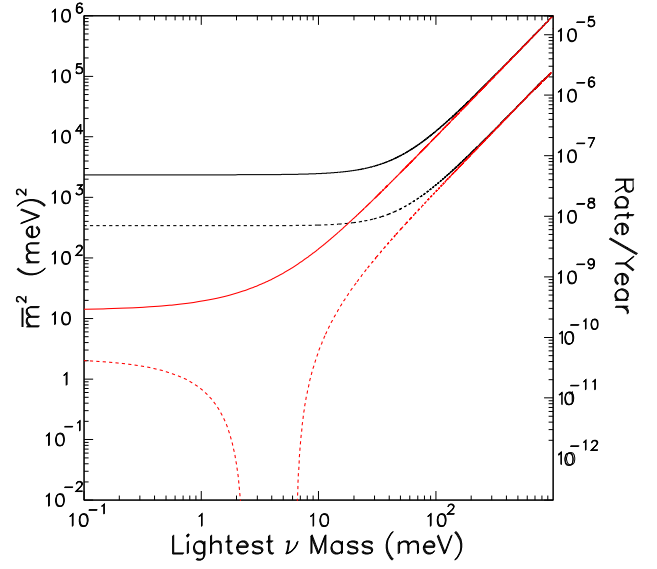


FIG. 4: Full range of  $\bar{m}^2$  for the normal and inverted hierarchies. The solid curves show the same curves labelled “coherent” in Fig. 3, while the dashed curves show the maximal destructive interference from possible Majorana phases. The scale on the right shows the corresponding MDBD rate expected in a 100 g tritium target. The rate is proportional to the mass of the target to the 4/3 power.

long as the neutrino wavepacket travelling from source to target stays together. However, the different mass components of the wavepacket physically separate and destroy coherence at large distances owing to the mass dependence of their velocities,  $\delta v/c \sim \frac{1}{2} \Delta m_\nu^2 / E_\nu^2$  [15]. If the initial neutrino wavepacket is of length  $\ell$ , then decoherence takes place over distances  $L_{dec} \sim \ell E_\nu^2 / \Delta m_\nu^2 \sim \ell E_\nu L_{osc}$ , where  $L_{osc}$ , discussed above, is the length over which neutrino oscillations become significant. The estimate  $\ell E_\nu \sim 1$  nm-MeV [19] implies that  $L_{dec}$  is  $\sim 10^4 L_{osc}$ , or  $L_{dec} \sim 10^4 E_\nu (\text{MeV}) / \Delta m_\nu^2 (\text{eV}^2)$  m. A detailed discussion of decoherence over astrophysical distances must thus take flavor oscillations of the neutrino wave packets into account.

## B. Dependence of the MDBD rate on geometry

We next consider the rate of MDBD in a macroscopic sample of  $N$  atoms of  $X$  with uniform density  $n$ . For an ensemble of beta emitters, Eq. (24) implies the total rate of MDBD,

$$\mathcal{R}_{MDBD} = \int d^3r d^3r' \frac{n^2 \mathcal{K}}{4\pi |\vec{r} - \vec{r}'|^2} = \frac{N^2 \mathcal{K}}{4\pi} \left\langle \frac{1}{(\vec{r} - \vec{r}')^2} \right\rangle. \quad (31)$$

For isotropic scaling at fixed density, the rate scales as the fourth power of the linear size of the system, or  $N^{4/3}$ . On the other hand, the rate of  $0\nu\text{DBD}$  scales with  $N$ .

The detailed evaluation of the integral depends on the geometry of the target. It is readily evaluated for a spherical target of radius  $R$  by writing,

$$\int \frac{d^3r d^3r'}{(\vec{r} - \vec{r}')^2} = \int \frac{d^3k}{4\pi k} \left| \int d^3r e^{i\vec{k}\cdot\vec{r}} \right|^2 = 4\pi^2 R^4, \quad (32)$$

where we use  $\int d^3r e^{i\vec{k}\cdot\vec{r}} = (4\pi/k^3)(\sin kR - kR \cos kR)$ .

The total double beta decay rate for a spherical source<sup>3</sup> is then

$$\mathcal{R}_{\text{MDBD}} = \frac{9}{16\pi} \frac{N_T^2}{R^2} \mathcal{K}, \quad (33)$$

which shows explicitly the scaling with the size of the sample (at fixed density) as  $N^{4/3}$ .

### C. Estimate of $\mathcal{R}_{\text{MDBD}}$

We estimate  $\mathcal{R}_{\text{MDBD}}$  from Eq. (33) with (28). For tritium,

$$\mathcal{R}_{\text{MDBD}} = \frac{9}{64\pi^2} \frac{N_T^2}{R^2} \bar{m}^2 \bar{\sigma}_T^2 K_{\text{end}}; \quad (34)$$

with a 100 g sphere of tritium ( $N_T \simeq 2 \times 10^{25}$  nuclei),  $\mathcal{R}_{\text{MDBD}} \simeq 2.32 \times 10^{-5} (\bar{m}/1 \text{ eV})^2/\text{year}$ . It is instructive to compare this rate with the conventional neutrinoless double beta decay rates for various nuclei. No  $0\nu\text{DBD}$  events have been positively identified [5], and the most sensitive recent results include those on  $^{76}\text{Ge}$  [22, 23],  $^{136}\text{Xe}$  [24–26],  $^{130}\text{Te}$  [27],  $^{82}\text{Se}$  [28, 29], and  $^{100}\text{Mo}$  [30]. Table I lists the expected  $0\nu\text{DBD}$  rates for these nuclei with an exposure of 100 g-yr, assuming  $\bar{m} = 0.1 \text{ eV}$ . As we see in the Table, the tritium MDBD rate is four to five orders of magnitude lower than those expected for  $0\nu\text{DBD}$ . This difference reflects the much smaller  $Q=16.8 \text{ keV}$  value in tritium beta decay than in  $0\nu\text{DBD}$ , e.g.,  $Q = 2.04 \text{ MeV}$  for  $^{76}\text{Ge}$  and  $Q=2.46 \text{ MeV}$  for  $^{136}\text{Xe}$   $0\nu\text{DBD}$ .

To illustrate the importance of a large  $Q$  value, we compare MDBD for neutrons (where  $n \rightarrow p + e^- + \bar{\nu}_e$  followed by  $\nu_e + n \rightarrow p + e^-$ ) with tritium. In this double beta decay  $Q = 2 \times 0.782 \text{ MeV} = 1.564 \text{ MeV}$ . Furthermore  $\bar{\sigma}_n$  is a factor  $\sim 20$  larger than in tritium, which has comparable matrix elements. In a sample of 100 g of

neutrons occupying the spherical volume as would 100 g of tritium, the MDBD rate is a factor  $\sim 10^5$  larger than in a comparable sample of tritium. In fact, the MDBD rate for such a neutron sample is comparable to that in an equivalent sample of nuclei in  $0\nu\text{DBD}$ . Clearly though, it would be impossible to do such an experiment in a cloud of laboratory neutrons.<sup>4</sup>

A somewhat more realistic candidate nucleus to consider in searching for MDBD is  $^{11}\text{C}$ , which undergoes a  $\beta^+$  decay with a half life of 22.3 min. with a  $Q$  value of 1.98 MeV. We estimate that a 100 g spherical sample of  $^{11}\text{C}$ , which has a density  $2.2 \text{ g/cm}^3$ , and contains 3/11 of the number of atoms in a 100 g sample of tritium, would have a MDBD rate of  $5.14 \times 10^{-5}$  per year for  $\bar{m} = 0.1 \text{ eV}$ , as shown in Table I. This rate is significantly larger than the MDBD rate for tritium, but still lower than the rate for the  $0\nu\text{DBD}$  sources listed in Table I. As mentioned, the MDBD rate contains no uncertainties arising from the nuclear matrix elements, distinctly different from in  $0\nu\text{DBD}$ .

## IV. MDBD SIGNAL VS. BACKGROUND

### A. Electron distribution in MDBD

The characteristic feature of MDBD is that the sum of the two electron energies is just twice the total energy released in a single beta decay. The distribution of the electron pairs has the structure, in the limit of small neutrino mass,

$$\begin{aligned} d^2 N(E_e, E'_e) &\propto p_e E_e F(E_e) dE_e p'_e E'_e F(E'_e) dE'_e \\ &\times \int dE_\nu \delta(\Delta M - E_\nu - E_e) \delta(\Delta M + E_\nu - E'_e) \\ &= p_e E_e F(E_e) F(E'_e) dE_e p'_e E'_e dE'_e \\ &\times \delta(2\Delta M - E_e - E'_e). \end{aligned} \quad (35)$$

The  $E_\nu^2$  from the neutrino phase space is canceled by neutrino helicity factor  $1 - \beta^2 = (m_\nu/E_\nu)^2$ . Then the single electron distribution in MDBD has the form,

$$\frac{dN_e}{dK_e} \propto p_e E_e F(E_e) F(E'_e) p'_e E'_e, \quad (36)$$

where here  $E'_e = 2\Delta M - E_e$ .

This distribution, shown in Fig. 5 in terms of the electron kinetic energy  $K_e$  for tritium MDBD, is clearly symmetric about the single beta decay endpoint,  $K_e = K_{\text{end}}$ .

<sup>3</sup> We give the result for a spherical source only for illustration, ignoring the complication that electrons produced within a sufficiently large spherical sample rapidly lose energy traversing the source and cannot readily be detected. For such a reason, the PTOLEMY experiment [20] is aiming for two dimensional targets, using tritiated graphene. A realistic MDBD experimental design would similarly require a more planar geometry, at the cost of reducing the probability of a given antineutrino from the initial beta decay finding a target for inverse decay.

<sup>4</sup> On the other hand, a neutron star contains beneath its crust a stable liquid of order  $10^{57}$  neutrons in a  $\sim 10 \text{ km}$  sphere, which implies a geometric enhancement over MDBD in 100 g of tritium by a factor  $\sim 10^{53}$ . The rate of MDBD is, however, significantly suppressed by Pauli exclusion in both URCA and modified URCA processes, as well as by BCS pairing. Unfortunately there is no way apparent to distinguish such MDBD processes in neutron stars, even in their cooling.

Nucleus	$T_{1/2}$ for $\bar{m} = 0.1$ eV	Yield per 100 g-yr
$^3\text{H}$ (MDBD)	—	$2.3 \times 10^{-7}$
$n$ (MDBD)	—	$3.4 \times 10^{-2}$
$^{11}\text{C}$ (MDBD)	—	$5.1 \times 10^{-5}$
$^{76}\text{Ge}$ ( $0\nu\text{DBD}$ ) [22, 23]	$1.1 \times 10^{26} < T_{1/2} < 6.0 \times 10^{26}$ yr	$9.1 \times 10^{-4} < Y < 5.0 \times 10^{-3}$
$^{136}\text{Xe}$ ( $0\nu\text{DBD}$ ) [24–26]	$3.0 \times 10^{25} < T_{1/2} < 5.6 \times 10^{26}$ yr	$5.5 \times 10^{-4} < Y < 1.0 \times 10^{-2}$
$^{130}\text{Te}$ ( $0\nu\text{DBD}$ ) [27]	$1.8 \times 10^{25} < T_{1/2} < 2.0 \times 10^{26}$ yr	$1.6 \times 10^{-3} < Y < 1.8 \times 10^{-2}$
$^{82}\text{Se}$ ( $0\nu\text{DBD}$ ) [28, 29]	$3.2 \times 10^{25} < T_{1/2} < 2.3 \times 10^{26}$ yr	$2.3 \times 10^{-3} < Y < 1.6 \times 10^{-2}$
$^{100}\text{Mo}$ ( $0\nu\text{DBD}$ ) [30]	$1.4 \times 10^{25} < T_{1/2} < 4.3 \times 10^{25}$ yr	$9.7 \times 10^{-3} < Y < 3.0 \times 10^{-2}$

TABLE I: Expected yields,  $Y$ , for MDBD and  $0\nu\text{DBD}$  for a 100 g-yr exposure using various nuclei. We assume the Majorana neutrino effective mass  $\bar{m} = 0.1$  eV. The uncertainties in the predicted  $T_{1/2}$  and yield for  $0\nu\text{DBD}$  reflect the range of uncertainties of the nuclear matrix elements adopted by Ref. [5] to relate the current experimental limits on  $T_{1/2}$  to values of  $\bar{m}$ . For MDBD we assume 100 g spherical sources of tritium (and neutrons, for illustration) with density  $1 \text{ g/cm}^3$  and  $^{11}\text{C}$  with density  $2.2 \text{ g/cm}^3$ .

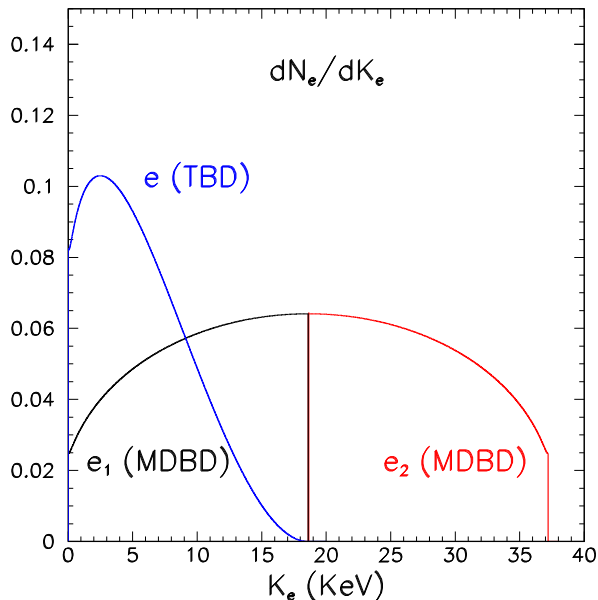


FIG. 5: The electron distributions in single tritium beta decay and in tritium MDBD, where  $e_1$  is the lower energy and  $e_2$  the higher energy electron. Here  $e_1$  is the electron produced in the initial beta decay, and  $e_2$  the electron emitted in the final inverse beta decay. The detailed structure of the single electron energy distributions at  $K_{\text{end}}$ , shown as a single vertical line, is in fact two curves separated essentially by  $2m_\nu$ , too fine to be seen in the figure.

The figure shows for comparison the electron distribution from single beta decay, which vanishes near  $K_{\text{end}}$ , as we see from Eq. (12), essentially as

$$\frac{dN_e}{dK_e} \propto \frac{d\Gamma}{dE_e} = \frac{\bar{\sigma}(E_e)}{2\pi^2} (\Delta M - m_e - K_e)^2; \quad (37)$$

the distribution is dominated by electrons emitted with a right handed neutrino. In this figure, we normalize the individual distributions to unity, and take the

Fermi Coulomb correction to be  $2\pi\eta/(1 - e^{-2\pi\eta})$  with  $\eta = Ze^2/v_e$ . The non-zero neutrino mass leads to a falloff of the  $e_1$  distribution at  $K_{\text{end}} - m_\nu$  and a rise of the  $e_2$  distribution at  $K_{\text{end}} + m_\nu$ , too fine a structure to see in the figure.

## B. Background

Although the signal for a macroscopic neutrinoless double beta decay is that the sum of the energies of the two electrons in the event is precisely  $2K_{\text{end}}$ , it would seem, given the high rates of single beta decay, that the challenge of separating the signal from the background is insurmountable. The  $2 \times 10^{25}$  tritons in 100 g of tritium, with a half-life of 12.3 years, would produce  $\sim 2.5 \times 10^{16}$  decays per second. However, only a tiny fraction of the decays give electrons with energy near the beta decay endpoint. An analogous challenge to separate the signal from the background is encountered in the proposed detection of relic neutrinos using the ITBD reaction [20, 31], where the signals are separated from the endpoint by twice the neutrino mass. Long et al. [16] show that an energy resolution better than  $0.7 m_\nu$  is sufficient to reach a signal to background ratio better than 1.

The signal to noise ratios for MDBD should be much better than in relic neutrino detection, and do not require superb energy resolution. As shown in Fig. 5, one of the two electrons from MDBD has an energy greater the endpoint energy of TBD, and up to twice the endpoint energy. By requiring that the more energetic electron from the MDBD candidate event has an energy sufficiently higher than the endpoint energy, the background can be rejected at only a small cost to the MDBD detection efficiency.

The favorable background rejection capability of MDBD is further illustrated in Fig. 6a, where the axes are the individual electron kinetic energies. An MDBD event would appear as a point on the diagonal line



$K_1 + K_2 = \Delta M - 2m_e$  in this figure. The MDBD accidental background from two electrons emitted in two independent single beta decays would lie in the red box in the figure, and except at the single point where the red square touches the straight line, the background is separated from the two electron MDBD event. The background from the upper-right corner of the square in Fig. 6a can be readily rejected by requiring that the MDBD candidate events are well separated from this corner.

By contrast, the background in the  $0\nu$ DBD reaction is from the  $2\nu$ DBD reaction. The two electron kinetic energies from the  $2\nu$ DBD background can reach the diagonal signal line in  $0\nu$ DBD everywhere, as shown by the red triangle in Fig. 6b. These  $2\nu$ DBD background events cannot be rejected without a significant loss of detection efficiency for the  $0\nu$ DBD signals, unless superb energy resolution is achieved.

The time separation between the two electrons can also be used to reject accidental background in MDBD. The two electrons from an MDBD event occur in a narrow time window, the travel time from source to target,  $\delta t \sim R/c$ , which can be of order tens of picoseconds, while the electrons from single beta decays are uncorrelated in time. In contrast the  $2\nu$ DBD background in  $0\nu$ DBD cannot be rejected on the basis of time separation.

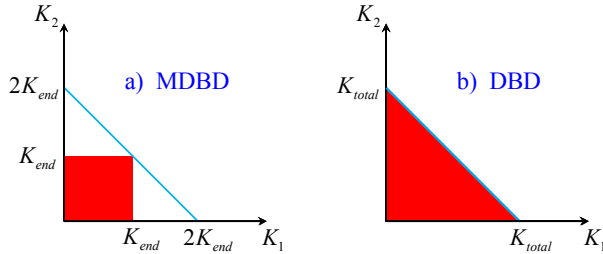


FIG. 6: The energy spectrum of two-electron events, with background in red, in a) MDBD and b)  $0\nu$ DBD. The axes are the kinetic energies of the individual electrons. The kinetic energies of the two electrons in both neutrinoless double beta decays lie along the (blue) diagonal line extending from the first electron having  $K_{total}$  (with  $K_{total} = 2K_{end}$  in MDBD) and the second with 0, to the reverse. The energies of two electrons produced in single beta decays, the background in MDBD, lie in the red box in a), reaching the diagonal line only at a single point. In contrast, in  $0\nu$ DBD experiments the background from double beta decay with neutrinos lies in the red triangle in b), coming up to the diagonal line everywhere.

## V. CONCLUSION

While neutrinoless double beta decay of single nuclei is the most promising experimental tool for testing the fundamental question of the Dirac or Majorana nature of neutrinos, the process of macroscopic neutrinoless double beta decay we have introduced here is another manifestation of Majorana neutrinos with non-zero mass. The

MDBD process shares features in common with single nucleus neutrinoless double beta decay; both depend on neutrinos being massive and Majorana, and both are affected by quantum interference between different neutrino mass states. The two processes have significant differences, however, including the absence of nuclear matrix element uncertainties for the MDBD rate and the different nature of the experimental backgrounds in these two processes. In addition MDBD exhibits the new phenomenon of quantum coherence over macroscopic distances, related, but not equivalent to neutrino oscillations.

Macroscopic double beta decay combines the processes of beta decay – as is being studied for tritium in the KATRIN [32] experiment for measuring the neutrino mass – and capture of neutrinos, as in the PTOLEMY experiment [20] to detect primordial neutrinos from the Big Bang. The MDBD process combining these two processes, could in principle be accessible in either of these two experiments. Our detailed analysis of various characteristics of MDBD, including expected rates, makes it clear that, given the quantities of tritium present, MDBD events are too rare to be detectable in the two experiments.

Nor is MDBD a viable alternative, at this point, to the well established neutrinoless double beta decay experiments to test the Majorana nature of neutrinos. We do not present MDBD as a currently feasible experiment. Nevertheless, the similarities and distinct differences between these two processes provide useful perspectives on the underlying mechanisms for these two processes, and indicate new directions in which the concept of MDBD can be explored.

An example, as mentioned earlier, is the analog of MDBD that can occur with emission of a Majorana antineutrino with a flavor  $\alpha$  other than electron, e.g., in  $\pi^- \rightarrow \mu^- + \bar{\nu}_\mu$ . The amplitude for capture of the emitted antineutrino on a nucleus as an electron neutrino would be proportional to  $\sum_i U_{\alpha i} U_{ei} m_{\nu i}$ , which is non-zero even if no phases enter the  $U_{\alpha i}$ . Such conversion of a Majorana  $\bar{\nu}_\mu$  into a  $\nu_e$  cannot occur in neutrinoless double beta decay within a single nucleus, simply by energy conservation, but can occur macroscopically.

## Acknowledgments

We thank Prof. Frank Deppisch and Dr. V. I. Tretyak for bringing the early work of A. F. Pacheco to our attention. This research was supported in part by the NSF Grant No. PHY-1812377 and by the Japan Science and Technology Agency (JST) as part of the Adopting Sustainable Partnerships for Innovative Research Ecosystem (ASPIRE), Grant Number JPMJAP2318, and was carried out in part at the Aspen Center for Physics, which is supported by National Science Foundation grant PHY-2210452, and at the National Central University in Taiwan under the Yushan Fellow Program.

- 
- [1] H. Primakoff and S. P. Rosen, Double beta decay, *Rep. Prog. Phys.* **22**, 121 (1959).
- [2] M. J. Dolinski, A. W. P. Poon, and W. Rodejohann, Neutrinoless double-beta decay: status and prospects, *Annu. Rev. Nucl. Part Sci.* **69**, 219 (2019).
- [3] S. R. Elliott and P. Vogel, Double beta decay, *Annu. Rev. Nucl. Part. Sci.* **52**, 115 (2002).
- [4] M. Agostini, G. Benato, J. A. Detwiler, J. Menéndez, and F. Vissani, Toward the discovery of matter creation with neutrinoless  $\beta\beta$  decay, *Rev. Mod. Phys.* **95**, 025002 (2023).
- [5] A. Barabash, Future beta decay experiments: recent achievements and future prospects, *Universe* **9**, 290 (2023).
- [6] A. Balantekin and B. Kayser, On the properties of neutrinos, *Annu. Rev. Nucl. Part Sci.* **68**, 313 (2018).
- [7] A. F. Pacheco, Neutrinoless double beta decay between pairs of single-beta emitters, *Phys. Rev. Lett.* **53**, 979 (1984).
- [8] Y. Kohyama, K. Kubodera, and K. Yazaki, Comment on neutrinoless double-beta decay between pairs of single-beta emitters, *Phys. Lett. B* **168**, 21 (1986).
- [9] M. Skalsey, Feasibility of detecting neutrinoless double-beta decay between pairs of single-beta emitters, *Phys. Rev. C* **36**, 820 (1987).
- [10] W. C. Haxton and G. J. Stephenson, Double Beta Decay, *Prog. Part. Nucl. Phys.* **12**, 409 (1984).
- [11] J. Engel and J. Menéndez, Status and Future of Nuclear Matrix Elements for Neutrinoless Double-Beta Decay: A Review, *Rep. Prog. Phys.* **80**, 046301 (2017).
- [12] J. Schechter and J. F. Valle, Neutrinoless double- $\beta$  decay in  $SU(2)\times U(1)$  theories, *Phys. Rev. D* **25**, 2951 (1982).
- [13] M. Duerr, M. Lindner, and A. Merle, On the Quantitative Impact of the Schechter-Valle Theorem, *JHEP* **1106**:091 (2011).
- [14] G. Baym and J. C. Peng, Evolution of Primordial Neutrino Helicities in Cosmic Gravitational Inhomogeneities, *Phys. Rev. D* **103**, 123019 (2021).
- [15] G. Baym and J. C. Peng, Evolution of Primordial Neutrino Helicities in Astrophysical Magnetic Fields and Implications for their Detection, *Phys. Rev. Lett.* **126**, 191803 (2021).
- [16] A. J. Long, C. Lunardini, and E. Sabancilar, Detecting non-relativistic cosmic neutrinos by capture on tritium: phenomenology and physics potential, *J. Cosm. and Astropart. Phys. JCAP* **1408**, 038 (2014).
- [17] R. G. H. Robertson and D. A. Knapp, Direct Measurements of Neutrino Mass, *Annu. Rev. Nucl. Part. Sci.* **38**, 185 (1988).
- [18] J. C. Peng and G. Baym, Inverse tritium beta decay with relic neutrinos, solar neutrinos, and a  $^{51}\text{Cr}$  source, *Phys. Rev. D* **106**, 063018 (2022).
- [19] B. J. P. Jones, E. Marzec, and J. Spitz, Width of a beta-decay-induced antineutrino wave packet, *Phys. Rev. D* **107**, 013008 (2023).
- [20] E. Baracchini et al., PTOLEMY: A Proposal for Thermal Relic Detection of Massive Neutrinos and Directional Detection of MeV Dark Matter; arXiv:1808.01892; M. G. Betti et al. (PTOLEMY Collaboration), Neutrino physics with the PTOLEMY project: active neutrino properties and the light sterile case, *JCAP* **07**, 047 (2019), arXiv:1902.05508 [astro-ph.CO].
- [21] X. Qian and J. C. Peng, Physics with Reactor Neutrinos, *Rep. Prog. Phys.* **82**, 036201 (2019).
- [22] I. J. Arnquist et al. (Majorana Collaboration), Final Result of the Majorana Demonstrator's Search for Neutrinoless Double- $\beta$  Decay in  $^{76}\text{Ge}$ , *Phys. Rev. Letters* **130**, 062501 (2023).
- [23] M. Agostini et al. (GERDA Collaboration), Final Results of GERDA on the Search for Neutrinoless Double- $\beta$  Decay, *Phys. Rev. Letters* **125**, 252502 (2020).
- [24] S. Abe et al. (KamLAND-Zen Collaboration), Search for the Majorana Nature of Neutrinos in the Inverted Mass Ordering Region with KamLAND-Zen, *Phys. Rev. Letters* **130**, 051801 (2023).
- [25] E. Aprile et al. (XENON Collaboration), Double-weak decays of  $^{124}\text{Xe}$  and  $^{136}\text{Xe}$  in the XENON1T and XENONnT experiments, *Phys. Rev. C* **106**, 024328 (2022).
- [26] G. Anton et al. (EXO-200 Collaboration), Search for Neutrinoless Double- $\beta$  Decay with the Complete EXO-200 Dataset, *Phys. Rev. Letters* **123**, 161802 (2019).
- [27] D. Q. Adams et al. (CUORE Collaboration), Search for Majorana neutrinos exploiting millikelvin cryogenics with CUORE, *Nature* **604**, 53 (2022).
- [28] G. Anton et al. (CUPID Collaboration), Final result on the neutrinoless double beta decay of  $^{82}\text{Se}$  with CUPID-0, *Phys. Rev. Letters* **129**, 111801 (2022).
- [29] R. Arnold et al. (NEMO Collaboration), Final results on  $^{82}\text{Se}$  double beta decay to the ground state of  $^{82}\text{Kr}$  from the NEMO-3 experiment, *Eur. Phys. J. C* **78**, 821 (2018).
- [30] C. Augier et al. (CUPID Collaboration), Final results on the  $0\nu\beta\beta$  decay half-life limit of  $^{100}\text{Mo}$  from the CUPID-Mo experiment, *Eur. Phys. J. C* **82**, 1033 (2022).
- [31] S. Weinberg, Universal Neutrino Degeneracy, *Phys. Rev.*, **145**7 (1962).
- [32] M. Aker et al., New Constraint on the Local Relic Neutrino Background Overdensity with the First KATRIN Data Runs, *Phys. Rev. Lett.* **129**, 011806 (2022).

## Appendix A: Helicity and chirality eigenstates

Finite mass neutrinos can have positive in addition to negative helicity. Here we derive the decomposition of helicity eigenstates into chiral eigenstates.

The Dirac state of a left handed (negative helicity) neutrino of energy  $E$  and mass  $m$ , propagating in the  $+z$  direction say, is

$$u_{\nu L} = \sqrt{\frac{E+m}{2E}} \begin{pmatrix} 0, 1, 0, -\frac{p}{E+m}, 0 \end{pmatrix}^T \equiv (0, W_+, 0, -W_-)^T, \quad (\text{A1})$$

where  $T$  denotes the transpose, and  $W_{\pm} \equiv \sqrt{(E \pm m)/2E}$ . From  $W_+^2 + W_-^2 = 1$  and  $W_+ W_- = \beta_{\nu}/2$ , we have  $(W_+ \pm W_-)^2 = 1 \pm \beta_{\nu}$ , and

$$W_{\pm} = \frac{1}{2} \left( \sqrt{1+\beta} \pm \sqrt{1-\beta} \right). \quad (\text{A2})$$

Similarly, the state of a right handed (positive helicity) neutrino is

$$u_{\nu R} = \sqrt{\frac{E+m}{2E}} \left( 1, 0, \frac{p}{E+m}, 0 \right)^T \equiv (W_+, 0, W_-, 0)^T. \quad (\text{A3})$$

On the other hand, the  $\gamma_5$  eigenstates for spin up or down (denoted by arrows) along the  $z$ -direction are

$$u_{\pm\uparrow} = \frac{(1, 0, \pm 1, 0)^T}{\sqrt{2}}, \quad u_{\pm\downarrow} = \frac{(0, 1, 0, \pm 1)^T}{\sqrt{2}}. \quad (\text{A4})$$

The helicity eigenstates can thus be written as

$$u_{\nu R} = \sqrt{\frac{1+\beta_\nu}{2}} u_{+\uparrow} + \sqrt{\frac{1-\beta_\nu}{2}} u_{-\uparrow}, \quad (\text{A5})$$

and

$$u_{\nu L} = \sqrt{\frac{1-\beta_\nu}{2}} u_{+\downarrow} + \sqrt{\frac{1+\beta_\nu}{2}} u_{-\downarrow}. \quad (\text{A6})$$

The amplitude for a  $\gamma_5 = \pm 1$  eigenstate to have right handed helicity is  $\sqrt{(1 \pm \beta_\nu)/2}$  and to have left handed helicity is  $\sqrt{(1 \mp \beta_\nu)/2}$ . The expectation value of the neutrino helicity  $\langle h \rangle$  in a  $\gamma_5 = \pm 1$  state is simply  $\pm \beta_\nu$ .